Large-amplitude compressive "sawtooth" magnetic field oscillations in the Martian magnetosphere

J. S. Halekas,[1] D. A. Brain,[1] and J. P. Eastwood[2]

Received 18 February 2011; revised 22 March 2011; accepted 25 April 2011; published 22 July 2011.

[1] We present Mars Global Surveyor mapping observations of large-amplitude "sawtooth" magnetic field oscillations in the induced magnetosphere of Mars and discuss their possible origin. These highly compressive, linearly polarized, quasiperiodic features occur above the sunlit hemisphere of Mars, below the magnetosheath, but outside of photoelectron-dominated regions. The correlation between solar zenith angle and estimated solar wind dynamic pressure at the sawtooth observation time and location at ~400 km altitude suggests an association with a flared boundary, possibly the ionopause. Magnetic reconnection, ionospheric instabilities and/or irregularities, and crustal magnetic field effects may all play a role in generating these compressional features, with individual observations suggesting that each may at times prove important. These processes each have implications for magnetospheric dynamics and nonthermal ion escape from the Martian system.

Citation: Halekas, J. S., D. A. Brain, and J. P. Eastwood (2011), Large-amplitude compressive "sawtooth" magnetic field oscillations in the Martian magnetosphere, *J. Geophys. Res.*, *116*, A07222, doi:10.1029/2011JA016590.

1. Introduction

[2] Mars, unlike the Earth, currently has no active dynamo and thus no global magnetic field capable of excluding solar wind plasma. At Mars, ionized atmospheric constituents instead provide the primary obstacle to the solar wind, forming an induced magnetosphere with a draped magnetic topology similar in many ways to that of Venus or comets. The Martian magnetosphere also has similarities to the terrestrial magnetosphere, including a bow shock, a magnetosheath, an ionosphere, and an extended wake region consisting of two oppositely directed magnetic lobes surrounding a hot plasma sheet region. However, at Mars the interplanetary magnetic field (IMF), rather than a planetary field, controls the orientation and topology of this magnetosphere. Furthermore, the relative contributions and spatial distributions of magnetic pressure and dynamic and thermal pressure from various ion species in the Martian magnetosphere differ greatly from the terrestrial case, resulting in physically different interaction regions and boundaries [*Nagy et al.*, 2004; *Dubinin et al.*, 2006, 2008a, 2008b]. At Mars, the main boundaries thus identified include (in descending order of altitude) a bow shock, a magnetic pileup boundary (MPB) where magnetic pressure increases to balance dynamic pressure (roughly collocated with the induced magnetospheric boundary (IMB) that separates solar wind from planetary ions), and a photoelectron boundary (PEB) below which atmospheric photoelectrons dominate over solar wind electrons (roughly collocated with the ionopause, at least at some times [*Duru et al.*, 2009]). These boundaries, each varying from extended and blurred to sharp and distinct depending on location and plasma conditions, clearly differ in many details from any analogous boundaries in the terrestrial magnetosphere. Therefore, while many familiar plasma processes operate in the Martian magnetosphere, we expect their relative importance, spatial and temporal distribution, and dynamical evolution to differ from the terrestrial case.

[3] Mars, unlike Venus or comets, has rather strong but spatially localized remanent crustal magnetization [*Acuña et al.*, 1999]. The crustal sources produce fields with strengths reaching several hundred nT even at MGS mapping altitude of ~400 km, sufficient to significantly perturb the location of plasma boundaries [*Brain et al.*, 2005; *Dubinin et al.*, 2006, 2008b; *Duru et al.*, 2009]. They also produce local regions of closed magnetic field which can exclude plasma of external origin, as well as regions of open field (cusps) which can act as conduits for both plasma access or escape [*Mitchell et al.*, 2001; *Brain et al.* 2007], and which may provide locations favorable for reconnection between IMF and crustal magnetic field lines [*Krymskii et al.*, 2002]. As Mars rotates and presents different faces to the solar wind, and as IMF polarity and clock angle change, reconnection likely drives changes in magnetic topology [*Brain et al.*, 2007], producing a highly dynamic magnetospheric configuration.

[4] The resulting dynamic Martian environment contains a wide variety of wave-like and/or turbulent phenomena, ranging from low frequency magnetic waves [*Brain et al.*, 2002; *Espley et al.*, 2004] to mirror mode and magnetosonic waves [*Bertucci et al.* 2004] to quasiperiodic oscillations of unknown origin in both suprathermal and thermal

[1]Space Sciences Laboratory, University of California, Berkeley, California, USA.
[2]Blackett Laboratory, Imperial College London, London, UK.

0148-0227/11/2011JA016590

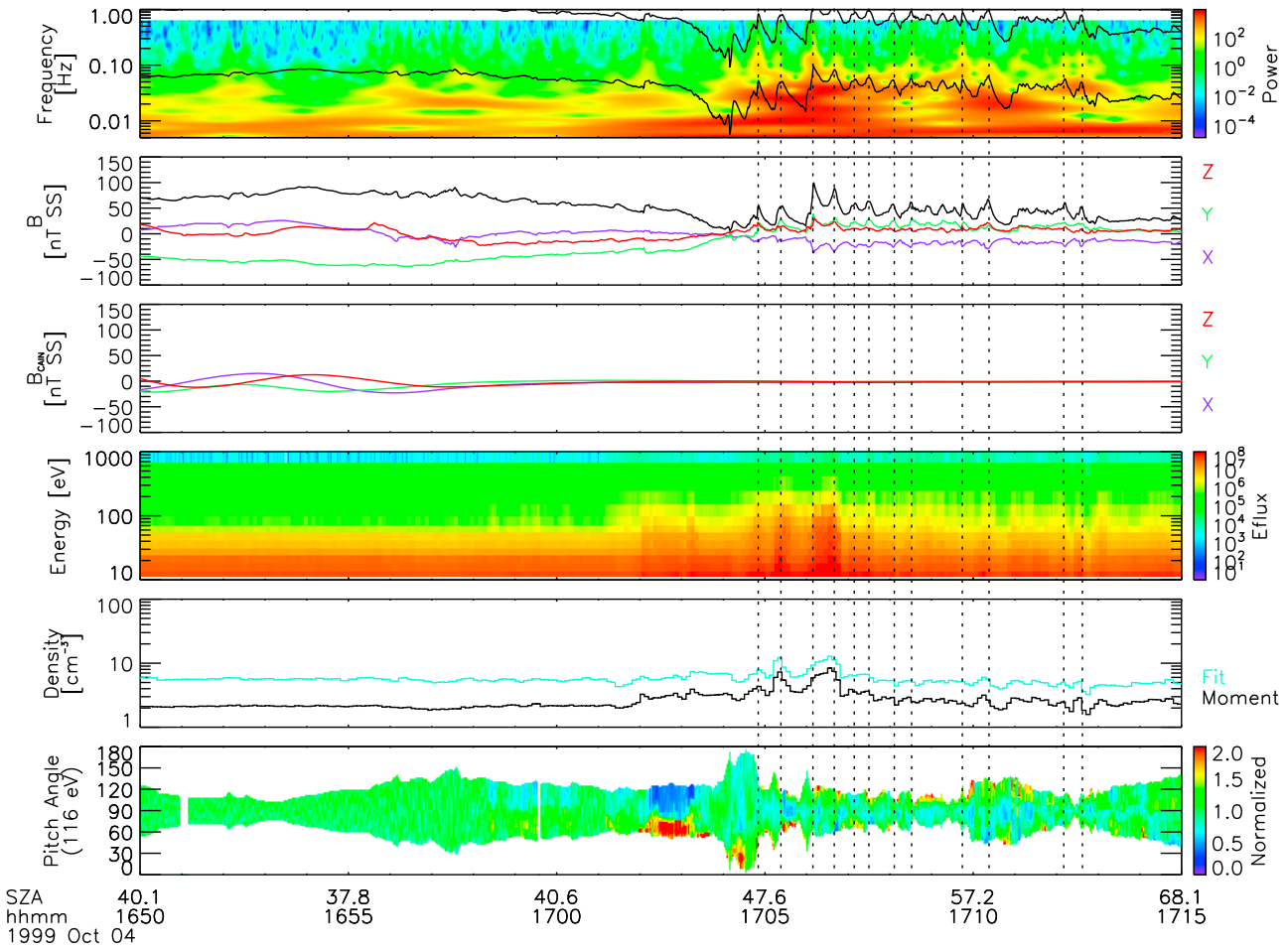

Figure 1. Overview of a sawtooth event on 4 October 1999 showing (from top to bottom) wavelet transform of magnetic field magnitude (black lines indicate oxygen and proton gyrofrequencies), magnetic field components and magnitude in sun-state coordinates, Cain model fields along the MGS orbit trajectory, electron energy-time spectrogram (eV/[cm^2 s sr eV]), approximate density from fits to a Maxwellian distribution (10–30 eV) and moment integrations (10–20,000 eV), and pitch angle spectrum for 116 eV electrons (normalized at each time to have an average value of unity, to better show anisotropies as a function of time). Labels on time axis indicate UT and spacecraft solar zenith angle. Dotted lines show the peaks of individual sawtooth oscillations.

plasma populations [*Winningham et al.*, 2006; *Gunell et al.*, 2008; *Gurnett et al.*, 2009]. Some of these phenomena, especially the latter observations, may result from shear-driven instabilities at the ionospheric boundary. In analogy with the Earth [*Otto and Fairfield*, 2000; *Fairfield et al.*, 2000] and Mercury [*Sundberg et al.*, 2010], one may plausibly expect to find the Kelvin-Helmholtz (KH) instability at Mars [*Amerstorfer et al.*, 2009; *Penz et al.*, 2004]; however, we do not yet know if this mechanism produces any of the observed phenomena, or its importance in the Martian magnetosphere if it does indeed operate there. If it does play a significant role at Mars, it could provide a mechanism for mixing of planetary and solar wind plasma, as well as an escape channel for planetary ions [*Penz et al.*, 2004]. Collisionless reconnection, recently observed at Mars by Mars Global Surveyor (MGS) [*Eastwood et al.*, 2008; *Halekas et al.*, 2009] provides another mechanism for plasma mixing and planetary ion escape, with observations indicating that flux ropes produced by reconnection between the IMF and crustal fields may prove a significant escape channel [*Brain et al.*, 2010].

[5] Processes driven by reconnection and/or ionospheric instabilities, and their control or lack thereof by crustal magnetic fields, may therefore provide a window on the relative importance and spatial distribution of important nonthermal ion escape channels. In this paper, we report on MGS observations possibly indicating such a phenomenon, in the form of highly compressive magnetic field oscillations, and discuss whether we can understand these observations in terms of reconnection or ionospheric instabilities partly controlled by crustal magnetic fields.

2. Observations of Large-Amplitude Compressive "Sawtooth" Oscillations

2.1. Data Set

[6] This study utilizes measurements made by the MGS Magnetometer and Electron Reflectometer (MAG/ER) instrument

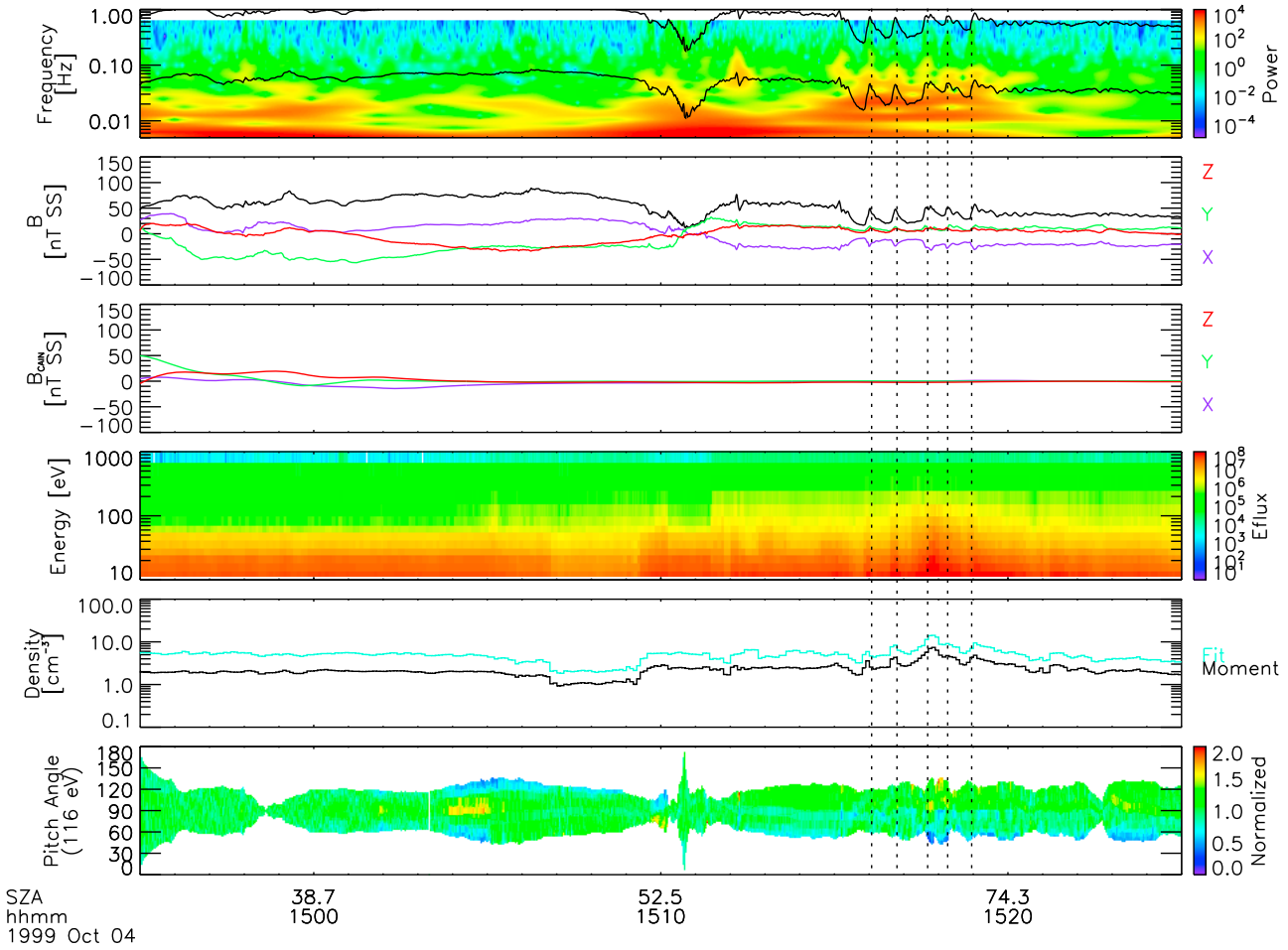

Figure 2. Overview of a sawtooth event on 4 October 1999 (one orbit before the event in Figure 1), in the same format as Figure 1.

[*Acuña et al.*, 2001; *Mitchell et al.*, 2001]. The MAG consisted of two identical fluxgate magnetometers, which provided fast vector measurements (up to 32 samples per second) of magnetic fields. The ER was a symmetric hemispherical "top hat" electrostatic analyzer, which measured the energy and angular distributions of 5 eV to 20 keV electrons, sampling thirty logarithmically spaced energy channels for sixteen 22.5° × 14° angular sectors spanning a limited 360° × 14° field of view on a three-axis stabilized spacecraft.

[7] In this study, we utilize data collected during the MGS mapping mission, extending from 1999 to 2006, during which MGS orbited at constant 14:00/02:00 local time and ~400 km altitude. Despite its constant altitude and local time, thanks to variability in plasma conditions MGS still samples many of the plasma regimes (and associated boundaries) discussed above, including the magnetosheath, the magnetic pileup region, and the photoelectron-dominated ionosphere. We study events identified both in the course of other investigations, and through a random search of the mapping data (as discussed in more detail in section 2.3 below).

2.2. Selected Observations

[8] We first discuss several representative examples of what we will call sawtooth oscillations, measured by MGS at 14:00 local time and ~400 km altitude. In Figures 1 and 2, we show magnetic field and electron data for the dayside portions of two consecutive orbits. The key observational characteristics of the sawtooth events are the very large-amplitude quasiperiodic oscillations in magnetic field strength (peaks indicated by dotted lines). The large changes in magnetic field amplitude, associated with correlated variations in all three of the vector components, indicate highly compressive and primarily linearly polarized oscillations. The oscillation frequencies lie near the Oxygen gyrofrequency (wavelets calculated using a Morlet transform with wave number 6, as suggested by *Espley et al.* [2004]), though this association may prove coincidental.

[9] These two events, and all others discussed in this paper, occur in sunlight, above the Martian dayside. We observe these events a moderate distance from strong crustal magnetic sources (as seen by the comparison with the Cain model [*Cain et al.*, 2003] estimate of uncompressed crustal magnetic field strength at the spacecraft location), and located downstream (as indicated by solar zenith angle). Current sheets, at ~17:04 and ~15:11 respectively, separate the crustal field regions and the sawtooth oscillations in both cases, suggesting that reconnection between IMF and crustal fields could play a role, as discussed in more detail in section 3.2.

[10] The suprathermal electrons also show signatures of the sawtooth oscillations for the events in Figures 1 and 2,

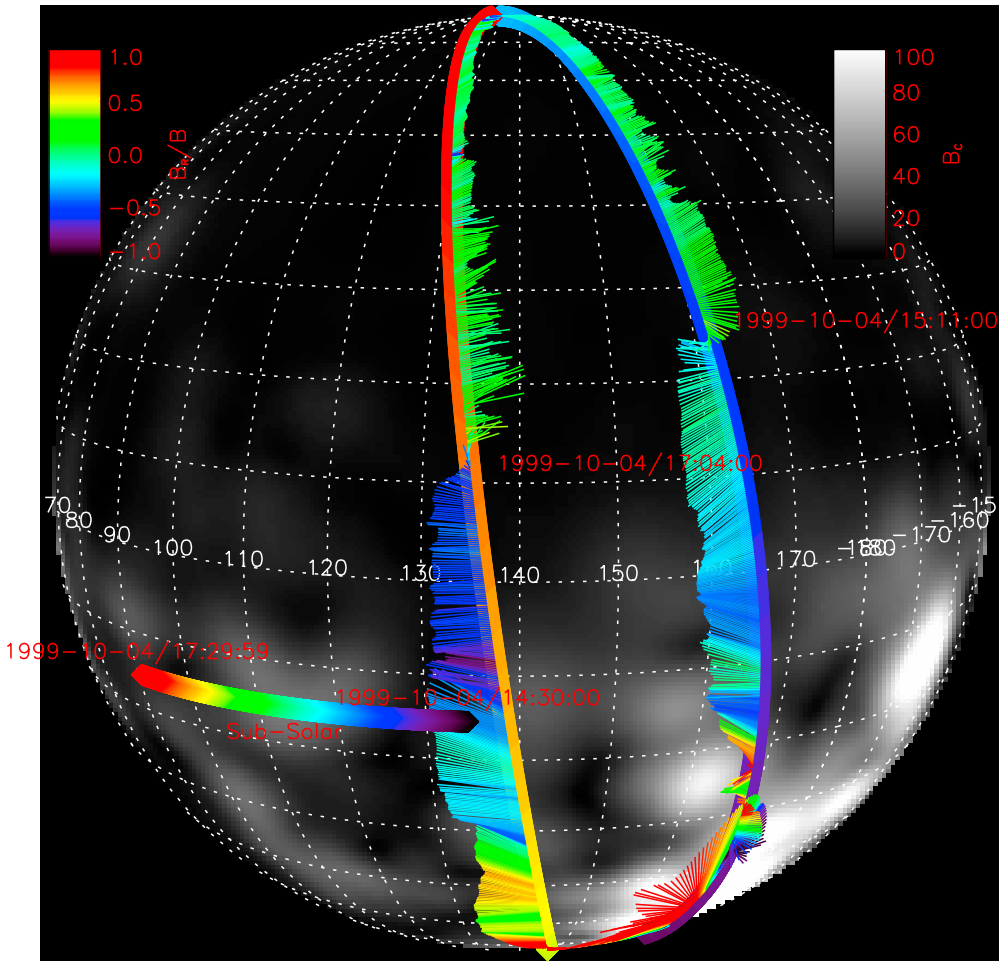

Figure 3. Magnetic field vectors for sawtooth events shown in Figures 1 and 2, with tangential components represented by whisker length and direction (originating from orbit track) and the radial component indicated by whisker color, as shown by color bar in upper left. The color of the orbit track indicates observation time, as indicated by the constant-latitude colored track on the surface, also showing the position of the subsolar point as a function of time. Grayscale background indicates strength of crustal field at orbital altitude, according to the Cain model, as shown by color bar in upper right.

with enhancements in suprathermal electron flux correlated with the magnetic field compressions. We calculate partial density moments both by direct integration and by fitting the low energy portion of the spectrum to a Maxwellian. These calculated partial densities have large systematic errors, given the incomplete electron energy coverage and lack of spacecraft potential information. In particular, the partial densities do not accurately capture the thermal electron contribution, and will therefore have especially large errors in the ionosphere. In the events of Figures 1 and 2, the partial densities calculated by fits and moments, though not agreeing in magnitude, agree in trend, consistent with density increases associated with magnetic compressions, suggesting magnetosonic compressional features. On the other hand, if most of the plasma density lies below the MGS measurement range, this interpretation may not hold.

[11] Before both example events, we observe relatively isotropic suprathermal electron distributions dominated by photoelectrons (as determined from energy spectra), consistent with a location below the PEB, possibly on closed magnetic field lines. For the event of Figure 1, these characteristics persist until 16:58, at which time we start to see more anisotropic electrons, with the suprathermal anisotropy and flux increasing at 17:02 and again at 17:04 as the sawtooth oscillations commence. Similarly, for the event in Figure 2, before 15:03 we observe mostly isotropic photoelectrons. Between 15:03 and 15:10, we see a suprathermal population consistent with a mix of photoelectrons and solar wind/sheath electrons, with loss cone distributions indicating likely magnetic connection to the collisional ionosphere and/or crustal fields. After 15:10, we observe a mostly isotropic suprathermal electron population, though some anisotropies appear at the peak of the sawtooth oscillations around 15:17. For both events, the flux and the anisotropy of the suprathermal electrons increase during the sawtooth events, and both quantities correlate with magnetic compressions. We observe anisotropies in both directions with respect to the field for the event in Figure 1, sometimes with alternating characteristics. These anisotropies might indicate fast electron flows along the field line (perhaps associated with reconnection), and/or electrons with an anisotropic temperature and a loss cone distribution, with the two possibilities

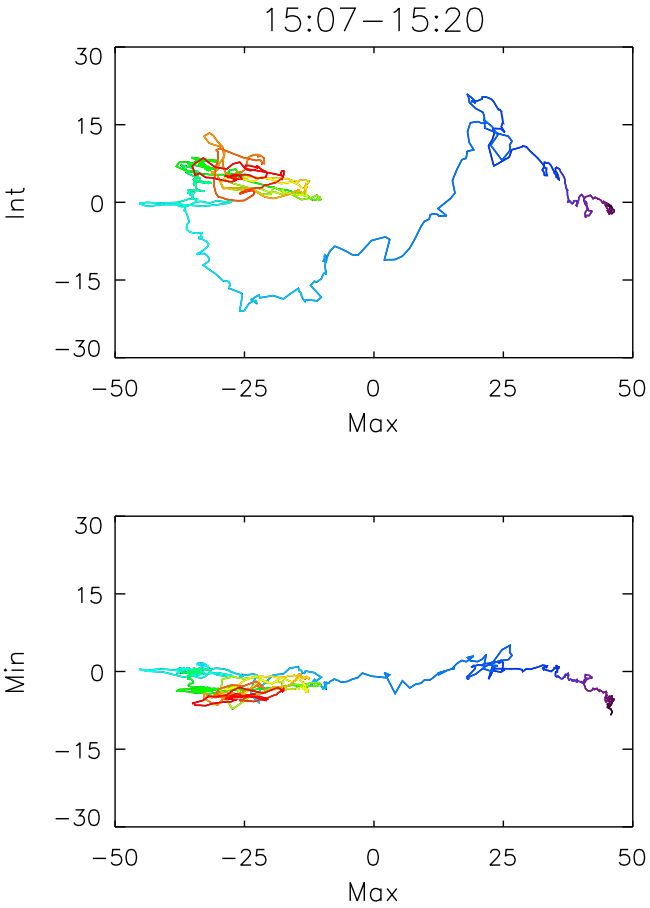

Figure 4. Magnetic field from sawtooth event shown in Figure 2, in minimum variance coordinates, with observation time indicated by color (purple, 15:07; red, 15:20). Purple to blue-green colors cover the time around the current sheet, while blue-green to red show the sawtooth oscillations, with all components in the same minimum variance coordinate system.

not easily distinguished by the limited angular coverage of MGS ER.

[12] We show magnetic field vectors for the events in Figures 1 and 2 in Figure 3. We find a very similar draping pattern on both orbits, with fields pointing westward and toward the Martian surface to the south of the current sheet, and eastward and nearly tangential to the surface to the north of the current sheet. The current sheet shifts in latitude by about 15° between the two observations, but the planetary longitude also rotates by 30° and shifts the location of crustal sources relative to the inflowing plasma commensurately, so one expects to find a somewhat modified picture, despite the constant local time of the MGS orbit. The large field component toward the surface just south of the current sheet supports a connection to crustal fields, while the tangential fields to the north of the current sheet follow the draping pattern expected for IMF field lines if the upstream IMF lies nearly in the ecliptic plane (as it most frequently should).

[13] For the event shown in Figure 2, we observe significant out of plane fields near the current sheet. We show these fields in more detail in minimum variance coordinates in Figure 4. Near the current sheet, we find the expected bipolar out-of-plane signature of Hall magnetic fields, consistent with a passage through a reconnection diffusion region (as previously observed above the Martian night side and flanks [*Halekas et al.*, 2009]). The nearly linearly polarized compressive sawtooth oscillations are first observed in the same plane as the main field component of the current sheet, and then rotate slightly out of this plane (still maintaining nearly the same minimum variance direction) as MGS travels farther from the current sheet crossing. The minimum variance direction (i.e., the current sheet normal) points almost radially out from the surface. Thus, MGS travels nearly parallel to the plane of the current sheet, passing through it tangentially.

[14] We next show a sawtooth observation with slightly different characteristics in Figure 5. This event has very similar magnetic field signatures to the events in Figures 1 and 2; however, we observe fewer changes in the suprathermal electrons. This indicates that, unlike the events in Figures 1 and 2, if significant plasma compression occurs, it only includes the unmeasured thermal electron component. We observe a photoelectron-dominated population before the event, until ~10:02. From ~10:02–10:12 we see a slightly anisotropic population with an energy spectrum consistent with a mix of photoelectrons and solar wind/sheath electrons. From ~10:12–10:18, MGS again enters a region dominated by isotropic photoelectrons, consistent with a location below the PEB. After ~10:18, including during the sawtooth oscillations, we observe a relatively featureless mixed population, with only a small anisotropy in suprathermal electron flux (more flux traveling sunward along the field line). In Figure 6, we show magnetic field vectors for the event in Figure 5. We find a magnetic rotation associated with the brief passage below the PEB just before the sawtooth oscillations, likely indicating an irregular ionospheric boundary, and suggesting a possible role for ionospheric instabilities, as discussed further in section 3.3.

[15] In Figure 7, we show a final example event with different characteristics from any of those described above. In the dayside southern hemisphere, we first pass through a region of isotropic photoelectron-dominated plasma from 8:57–9:03. From 9:03–9:18, we observe sawtooth oscillations, coincident with more energetic and anisotropic plasma, with increases in suprathermal electron density and anisotropy correlated with the magnetic compressions. From 9:18–9:31, we observe magnetic features with both compressional and rotational characteristics. These features, though not force-free flux ropes, may represent flux ropes either still in formation or out of equilibrium. Finally, near the north pole, at 9:50–9:53, we observe another burst of sawtooth oscillations. Figure 8 shows that, during most of the time period shown in Figure 7, tangentially draped field lines point either toward or away from a region of strong crustal fields near the subsolar point. Thus, these roughly tangentially draped fields, likely resulting from a north-south oriented upstream IMF, should interact with crustal fields near the subsolar point, subsequently affecting the flow of plasma laterally around the Martian ionosphere. The interaction of the IMF and crustal fields near the subsolar point may produce the flux rope like features from 9:18–9:31 (which travel with the

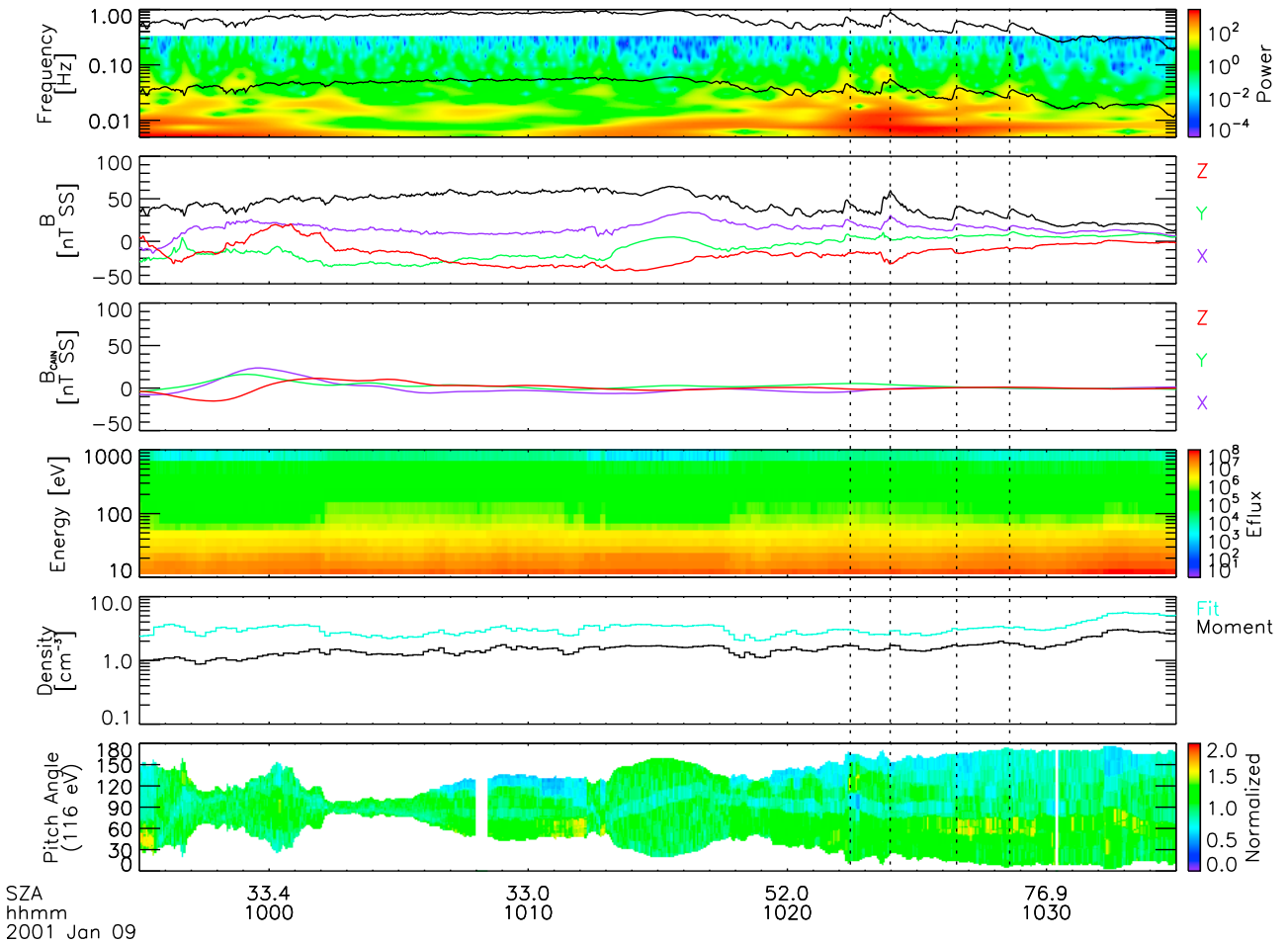

Figure 5. Overview of a sawtooth event on 9 January 2001, in the same format as Figure 1.

plasma eastward around the ionosphere), and may also indirectly generate the sawtooth oscillations in both the southern and northern hemispheres.

2.3. Statistical Distribution

[16] We found ~10 sawtooth events serendipitously (including those in Figures 1–3) in the course of other studies of the Martian environment. We then performed a systematic survey by randomly sampling 1000 ~2 h MGS orbits throughout the mapping mission, and found ~60 more sawtooth events. We also checked two orbits before and two orbits after each of the ~70 orbits in which we first found sawtooth oscillations, in many cases finding more events on consecutive orbits (for example, the cases shown in Figures 1 and 2). Indeed, we found repeated sawtooth signatures on successive orbits for ~40% of our examples, in a few cases for up to four consecutive orbits. This multistep search finally resulted in a data set of 112 sawtooth events. This does not represent a statistically unbiased sample of all sawtooth events, given the partially targeted search, but provides a sampling of the conditions and locations favorable for observation of sawtooth oscillations. Given the frequency of observations of sawtooth oscillations thus identified, we estimate a roughly 5% occurrence rate at 400 km altitude and 14:00 local time.

[17] We investigated all of the events in this data set, and found that all occur at a time and location characterized by electron distributions that do not have the signatures of either magnetosheath or photoelectron dominated plasma, implying a location below the MPB/IMB, and above the PEB (MGS can experience both the magnetosheath and ionosphere at mapping altitude, depending on plasma conditions, so this conclusion is meaningful). This consistency in event location argues for a formation mechanism operating in the Martian magnetosphere, and most likely below the magnetosheath, rather than farther upstream or outside of the bow shock.

[18] We investigated the resulting data set for any systematic biases that might indicate conditions favorable for formation of the sawtooth oscillations. Figure 9 shows the center location of observation of all 112 observations, in geographic coordinates. All observations lie in sunlight, and given the fact that MGS samples at a constant 14:00 local time, one can roughly relate geographic latitude to latitude relative to the sun. However, because of Mars' orbital obliquity of ~25°, the planet seasonally rocks relative to sun-state coordinates by this range of angles. We capture this variation by binning the data into three different ranges of subsolar geographic latitude, revealing seasonal effects. Sawtooth oscillations occur everywhere except over the

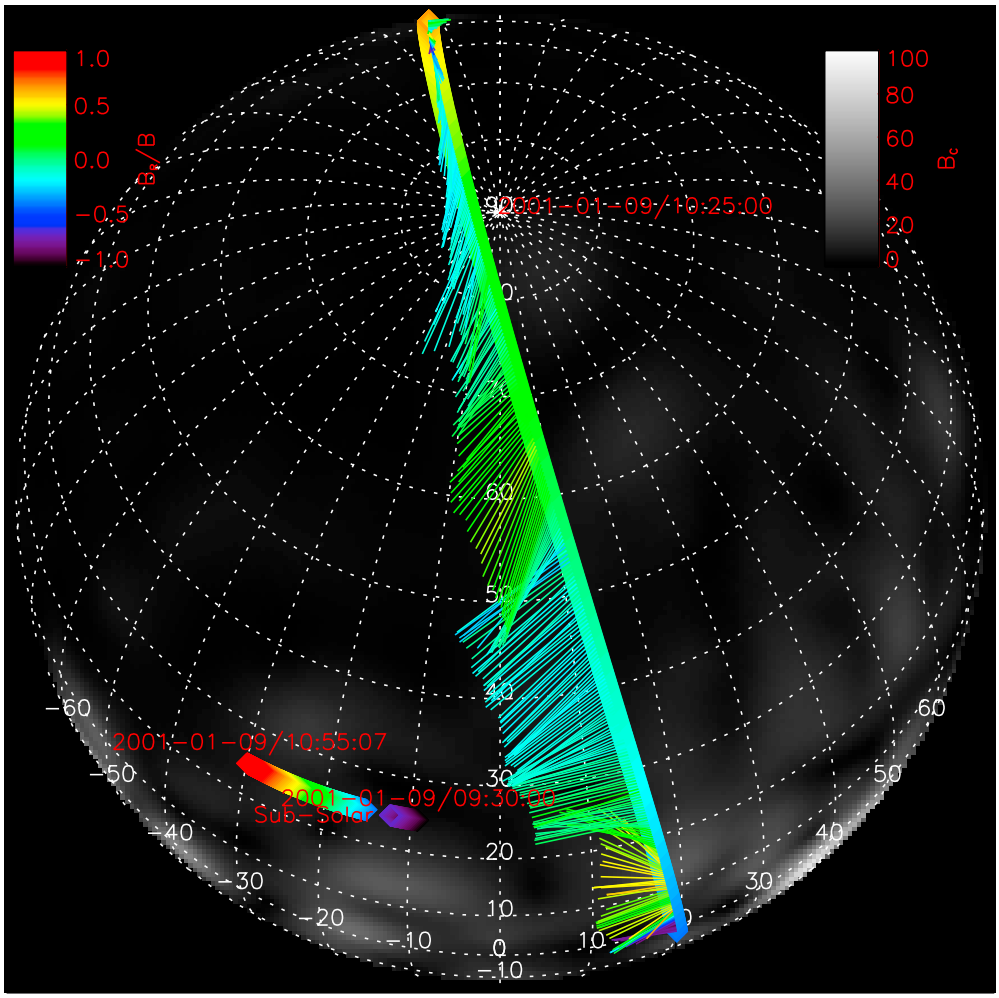

Figure 6. Magnetic field vectors for sawtooth event shown in Figure 5, in the same format as Figure 3.

strongest crustal fields, with the lack of observations possibly only reflecting the higher altitude of magnetospheric boundaries in these areas. At times with subsolar latitudes north of the equator (red events in Figure 9) we more often observe sawtooth events near the north pole or just south of and downstream from the belt of crustal fields around the equator. On the other hand, at times with subsolar latitudes south of the equator (black events in Figure 9) we more often observe them near the south pole or just north of and downstream from the equatorial crustal fields. This event distribution suggests that the position of the crustal fields relative to the subsolar point affects the likelihood of observing sawtooth oscillations. This may indicate that crustal fields affect the draped magnetic field topology in such a manner as to enhance the production of these features, or it may indicate that they perturb boundaries in such a way as to increase the likelihood of observing sawtooth oscillations at these locations at ~400 km altitude.

[19] In Figure 10, we show the distribution of subsolar magnetic field (extrapolated from a cos(SZA) fit to observed noncrustal field strength, producing a solar wind dynamic pressure proxy developed by *Brain et al.* [2005]) and the center SZA of the sawtooth observation. Compared to the average distribution for all mapping orbits, we find a slight preference for higher solar wind dynamic pressure, and a positive correlation between solar wind dynamic pressure and SZA at higher SZA. Recalling that increased solar wind dynamic pressure will compress interaction regions and lower the altitude of magnetospheric boundaries, we see that this distribution matches that expected for a flared boundary observed at a constant altitude, since higher dynamic pressure allows MGS (at a constant altitude) to sample a flared boundary at higher SZA. All boundaries in the Martian magnetosphere flare to some degree with SZA, as a natural consequence of pressure balance; however, the ionopause, with an average altitude of ~400–500 km, increasing to an average of ~600 km at high SZA [*Duru et al.*, 2009], has the most likely distribution of altitude versus SZA needed to match the trend in the observations. This naturally suggests that sawtooth oscillations result from instabilities at the ionospheric boundary, a possibility we explore in more detail in section 3.3.

[20] We also explored other parameters, including IMF draping direction, the change in IMF draping direction from orbit to orbit (a proxy for solar wind variability), and solar UV. We have not yet found any obvious difference in these parameters at times when we observe the sawtooth oscillations. However, we cannot measure any of these quantities

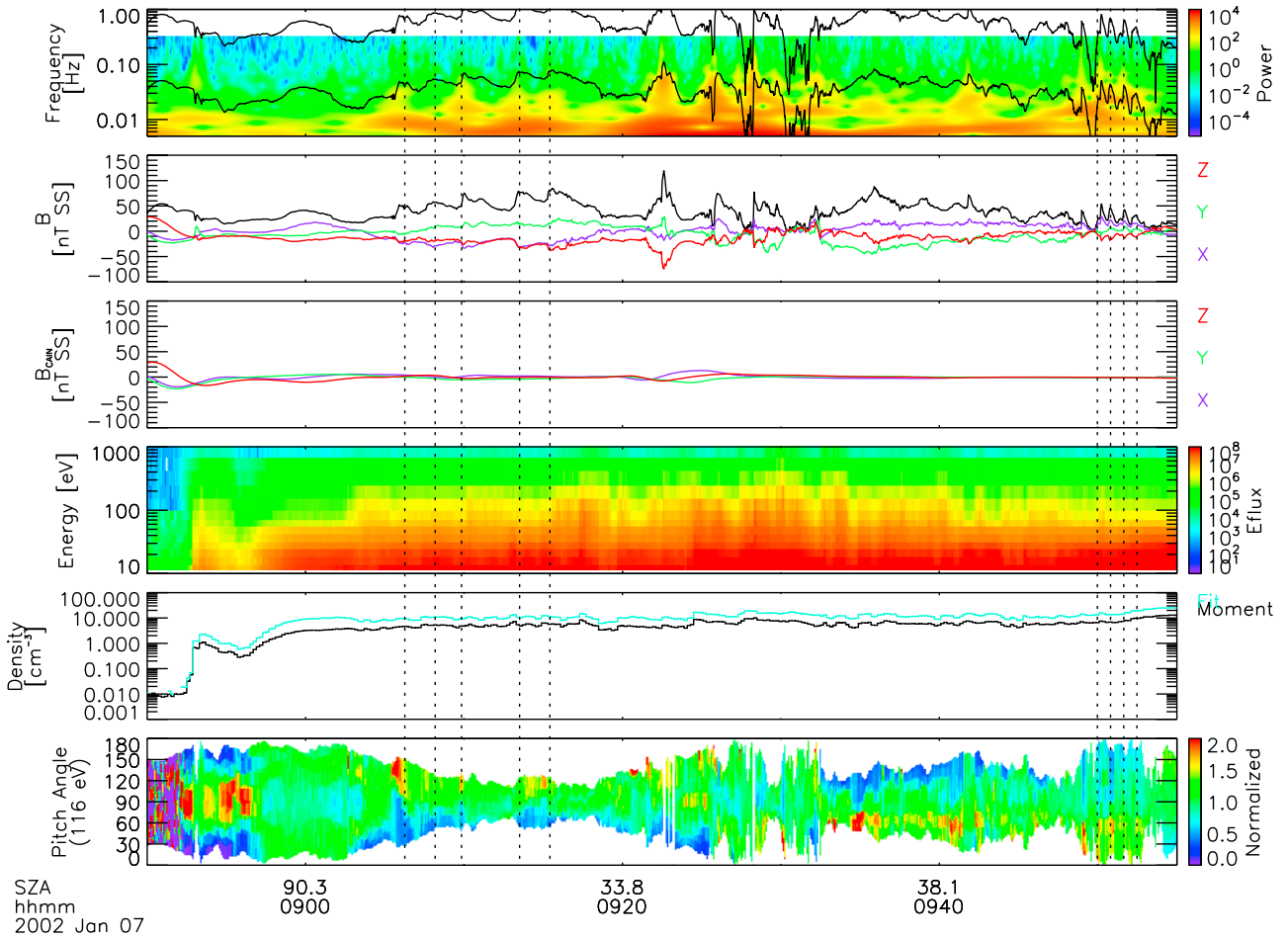

Figure 7. Overview of sawtooth events on 7 January 2002, in the same format as Figure 1.

directly, given our observation location and limited instrumentation, but instead must rely on extrapolations and proxies; therefore, we cannot necessarily conclude that these factors do not influence the sawtooth oscillations in some fashion. Indeed, these factors could couple to other inputs in ways that make it difficult to determine their influence on the sawtooth formation process. For instance, IMF direction might play a very important role if reconnection produces some of the sawtooth oscillations, but it would have a different relationship for each differently oriented crustal source, and for each rotational phase of Mars, producing a highly variable effect difficult to tease out of the data. For some events, as discussed in more detail in section 3.2, the data suggest that reconnection between the IMF and crustal fields may in fact prove important in just this fashion.

3. Discussion

3.1. Overview of Mechanisms for Sawtooth Formation

[21] In general, given the time-space ambiguity inherent in single spacecraft measurements, the sawtooth structures could represent several different types of phenomena (or a mix thereof), including temporal oscillations, stationary small-scale plasma structures that the spacecraft passes through, or large-scale plasma structures that move past the spacecraft at higher speed. In both examples shown here, and in every other case found to date, we observe steepening of the leading edge of the compressive oscillations, providing an important clue. For locally stationary structures, given similar observations in both hemispheres (i.e., at times with both sunward and antisunward spacecraft motion), we would expect to see a mix of steepening on the leading and trailing edges (in a temporal sense). Therefore, the consistent steepening observed on the leading edge in both hemispheres, sometimes on the same orbit (e.g., Figure 7), provides strong evidence against spatially stationary nonoscillatory structures. If correct, this implies that the sawtooth features most likely represent either local temporal oscillations or large-scale structures moving past the spacecraft. We have not yet identified a process that could locally produce stationary linearly polarized compressive oscillations steepened in this fashion. Therefore, relatively large structures moving past the spacecraft may provide the most plausible explanation for the observed sawtooth oscillations. Assuming the sawtooth structures move past the spacecraft at approximately the local plasma flow speed, most likely on the order of 10–50 km/s where they occur, their typical temporal duration of 30–60 s therefore corresponds to a spatial scale of ~300–3000 km, on the order of 0.1–1 Martian radii, and comparable to relevant ion scales. The observed steepening may reflect the

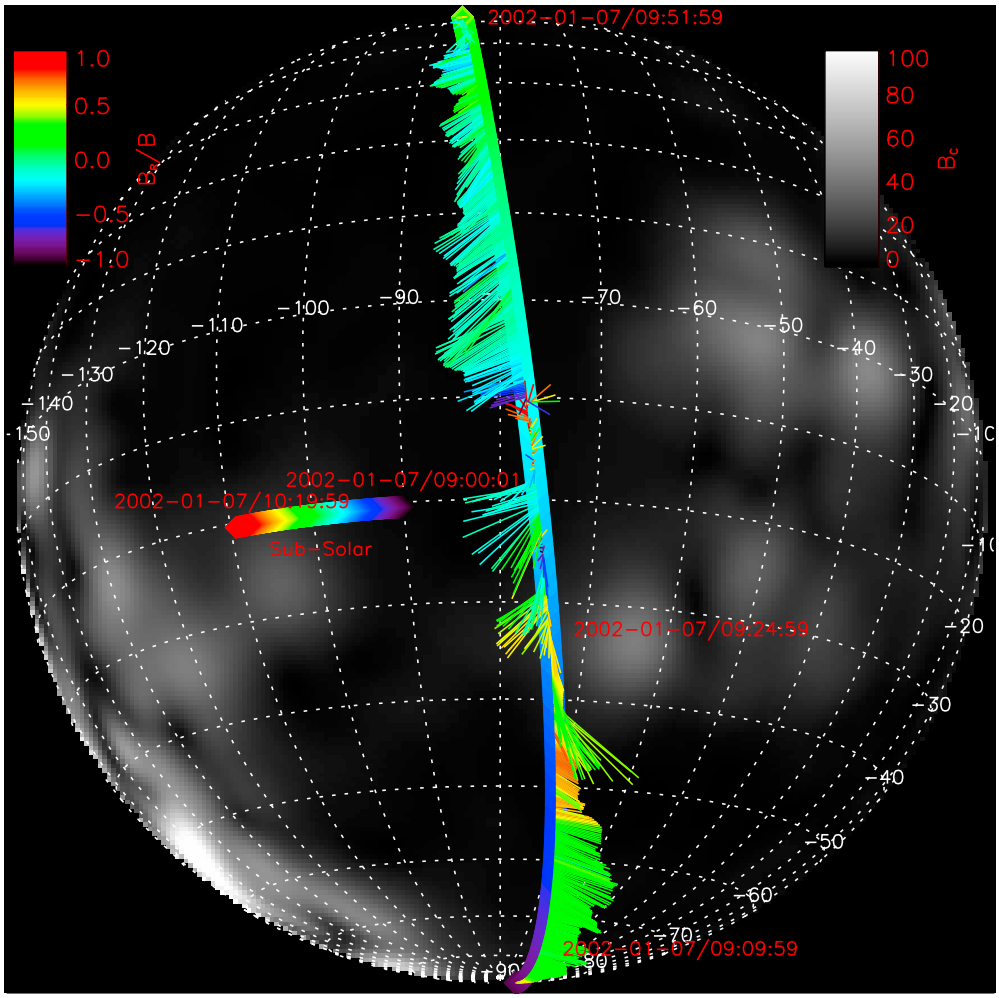

Figure 8. Magnetic field vectors for sawtooth events shown in Figure 7, in the same format as Figure 3.

condition of wave speed lower than flow speed (unlikely if magnetosonic in nature), or more likely the temporal evolution of the generation mechanism for the compressional features.

[22] We have considered a number of formation mechanisms and wave modes for the sawtooth oscillations. Clearly, magnetosonic waves provide a likely mode for the sawtooth oscillations, though the lack of measurements of the thermal plasma component below a few eV makes this conclusion necessarily only tentative. Even if this identification proves correct, though, we still must determine what process(es) drive the oscillations, and why the waves appear steepened in the spacecraft frame. No scenario conjectured thus far easily explains every observation, possibly indicating that multiple processes may operate (in concert?) to generate the sawtooth oscillations.

[23] A few characteristics of the sawtooth oscillations disfavor several formation mechanisms. Pickup ion produced waves, though supported by a rough association with the Oxygen gyrofrequency, appear unlikely given the highly linear polarizations observed. Though pickup ion waves can steepen to form compressive structures like those observed, for instance at comets [*Tsurutani et al.*, 1987], they still generally have a much more significant rotational component than the features observed here. Furthermore, analogous comet observations usually have leading wave trains of whistler mode turbulence, whereas we do not observe any precursors even in the highest time resolution (32 Hz) data available. We also considered the possibility of field line resonances; however, we can tentatively rule these out, given the anticorrelation of the distribution of observations with strong crustal fields. Finally, we considered the possibility of bi-ion shocklets produced in the sheath and/or upstream from the bow shock, as described by *Dubinin et al.* [1998], but these appear less likely given the observation location below the MPB.

3.2. The Role of Reconnection

[24] Reconnection provides one likely candidate to produce the sawtooth oscillations. MGS has observed reconnection in many locations of the Martian magnetosphere [*Eastwood et al.*, 2008; *Halekas et al.*, 2009] as well as large flux ropes likely produced by reconnection [*Brain et al.*, 2010]. While the direct observation of a flux rope would have rotational signatures inconsistent with our observations, episodic reconnection could provide impulses necessary to drive quasiperiodic compressions elsewhere. Reconnection could involve solar wind current sheets, or current sheets

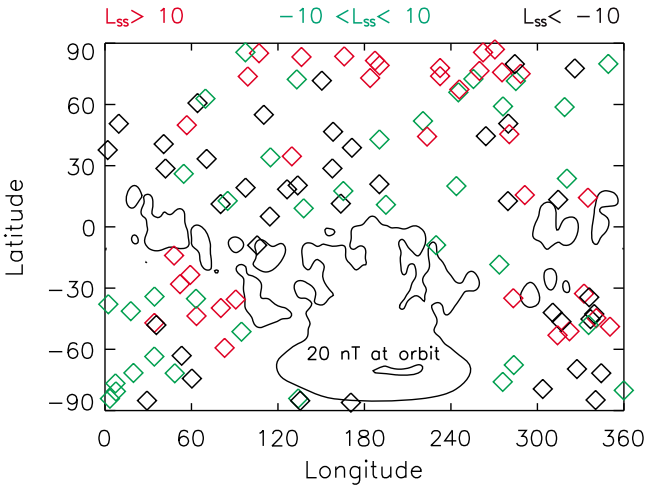

Figure 9. Distribution of sawtooth events in planetary coordinates, with 20 nT contour at orbital altitude (from Cain model), separated into three groups according to subsolar latitude L_{SS}.

between antiparallel draped IMF and crustal field lines, with observations supporting the latter scenario. We note that the events in Figures 1 and 2 both occur just downstream from current sheets that approximately separate regions of crustal magnetic fields dominated by nearly isotropic photoelectrons from regions dominated by draped IMF field lines and populated by a higher energy anisotropic suprathermal electron population. The existence of current sheets on successive orbits at nearly the same location argues against an origin related to solar wind discontinuities, and instead supports the interpretation of a current sheet formed between draped IMF and either distorted crustal magnetic field lines or IMF field lines entrained with and/or connected to crustal fields (the field in the south may even include a "fossil" field component emplaced in the ionosphere at an earlier time

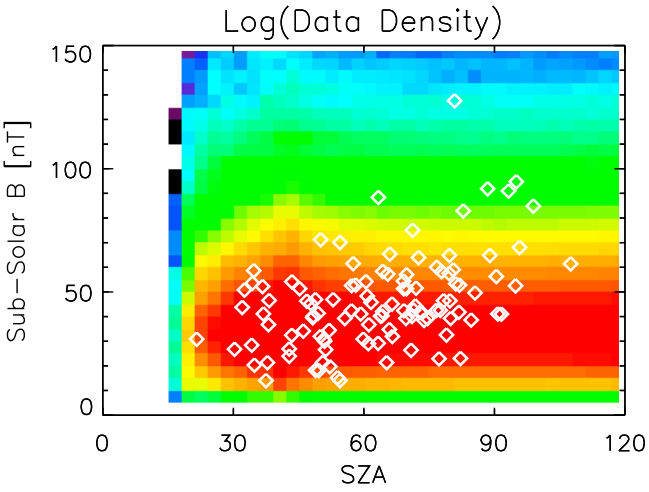

Figure 10. Distribution of sawtooth events in terms of solar zenith angle and solar wind dynamic pressure proxy (diamonds), overlaid on the overall data density for the entire MGS mapping mission.

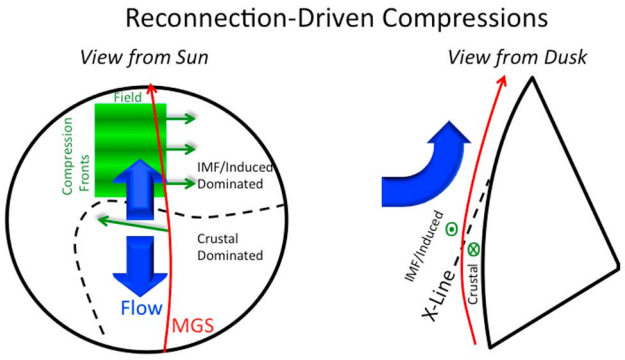

Figure 11. Schematic illustration of one possible explanation for sawtooth events shown in Figures 1–3, by pileup of IMF field and quasiperiodic release by reconnection with crustal-dominated fields at lower altitudes.

with a different IMF orientation, as observed recently at Titan [*Bertucci et al.*, 2008]).

[25] In order to interpret these observations, we consider the prevailing plasma flow in the Martian magnetosphere. Shocked solar wind plasma will flow tangentially around the ionosphere of Mars, carrying IMF field lines with it. The flow should stagnate at low altitudes above the subsolar point. At the location of MGS at ~400 km altitude, just north of the subsolar point, the flow should have a component northward and tangential to the surface, with some smaller component toward the surface. We show a cartoon of the field topology and plasma flow pattern we infer for these observations in Figure 11. The flow toward the planet, carrying IMF field lines with it, meets a crustal-field and photoelectron-dominated region. The plasma should mostly flow to the north and around the ionospheric obstacle. However, given the antiparallel field geometry, the almost radial current sheet normal, and the residual flow component toward the surface, conditions favorable for reconnection exist near the subsolar point. The field at the current sheet has only a small (unresolved by observation) normal component, indicating a relatively low reconnection rate (we estimate < ~10% given the uncertainties in the determination of the normal). Thus, reconnection likely can only convert a fraction of the incident magnetic flux, forcing much of the plasma to stagnate and/or flow laterally around the obstacle. If reconnection proceeds episodically, it could then lead to pileup and release of a portion of the draped field. Since we observe Hall magnetic fields characteristic of the reconnection diffusion region on one orbit, but not the next, episodic and/or spatially variable reconnection seems likely. Reconnection-driven pileup and release of compressed IMF could therefore plausibly produce the compressional features we observe as sawtooth oscillations.

[26] Reconnection could also plausibly produce the anisotropic suprathermal electron signatures often found with the sawtooth compressions. Previous studies have found evidence for similar anisotropic electron signatures near reconnection sites above the Martian night side and terminator [*Halekas et al.*, 2009], and similar features have been observed in the terrestrial magnetosphere. The anisotropic electrons may represent carriers of the Hall current and/or electrons accelerated outward from the reconnection site.

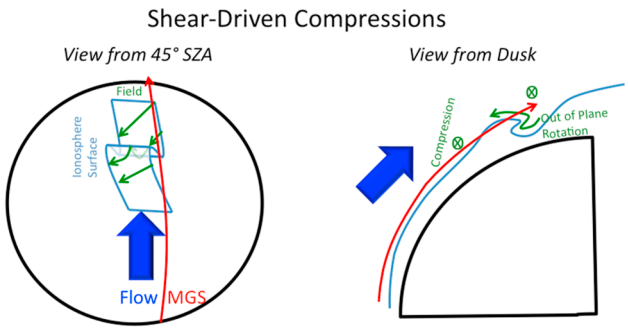

Figure 12. Schematic illustration of one possible explanation for sawtooth events shown in Figures 5 and 6, by pileup of IMF field above ionospheric irregularities produced by shear-driven instabilities.

3.3. The Role of Ionospheric Instabilities

[27] Ionospheric instabilities provide another natural candidate for generating the sawtooth oscillations, especially given the indications of an association with the ionopause discussed in section 2.3. As described by *Gurnett et al.* [2009], ionospheric instabilities can produce large dynamic effects at low altitudes in the ionosphere, which could drive processes at higher altitudes. In particular, any instability capable of producing a large irregularity in ionospheric structure could affect the transport of plasma at higher altitudes, perhaps leading to a pileup and release of compressed field capable of producing the quasiperiodic compressive features we see.

[28] In the MHD approximation, the onset condition for the KH instability has $[\mathbf{k}\cdot(\mathbf{v_1}-\mathbf{v_2})]^2 > \frac{n_1+n_2}{4\pi m n_1 n_2}[\mathbf{k}\cdot(\mathbf{B_1}+\mathbf{B_2})]^2$ [e.g., *Otto and Fairfield* [2000]. Finite Larmor radius effects [*Sundberg et al.*, 2010; *Penz et al.*, 2004; *Amerstorfer et al.*, 2009], gravitational forces [*Penz et al.*, 2004], and additional restoring terms from magnetic curvature can also play a role, but we can still think of the KH instability in terms of velocity shear overcoming a magnetic restoring force. If KH plays a significant role at Mars, it should therefore occur most often at high SZA near the ionospheric boundary (maximizing the velocity shear), for fields oriented tangential to the boundary and perpendicular to the flow (minimizing the restoring force). Much like at the Earth, one should then see KH at the "equatorial" flanks of the magnetosphere [*Fairfield et al.*, 2000], but with the "equator" at Mars corresponding to a magnetic rather than geographic location. In analogy to the Earth, we expect to see the observational hallmark of out of plane rotations perpendicular to the draped magnetic field, as the instability leads to "rolling up" of field vortices [*Otto and Fairfield*, 2000; *Fairfield et al.*, 2000].

[29] With this in mind, we revisit the sawtooth observation shown in Figures 5 and 6. We note that the passage below the PEB (also below the ionopause?) from ~10:12–10:18, observed just before and upstream from the sawtooth oscillations, occurs at the same time as an out of plane rotation of the draped magnetic field. The field points southwest (not quite perpendicular to the likely northward plasma flow), with a small component toward the surface, aligned roughly tangential to the expected ionospheric boundary, fairly favorable for the growth of the KH instability. However, the observed rotational feature covers about 20° in latitude, or ~1000 km, and appears fairly stable for the ~6 min it takes to traverse the structure. These values exceed the length scale and inverse of growth rate predicted by *Penz et al.*, [2004] by an order of magnitude, suggesting that the KH instability may not have formed at this particular time and location.

[30] However, this does not preclude an ionospheric instability producing the sawtooth oscillations that MGS later flies through, since the instability could still form at higher latitude and/or at a lower altitude. Indeed, velocity shear should increase at higher SZA, commensurately increasing the likelihood of KH instability growth where MGS observes the sawtooth oscillations. Regardless of whether a KH vortex fully develops or not, though, any ionospheric irregularity like that observed could affect plasma flow around the ionosphere, and lead to plasma pileup and magnetic field compression upstream from the vortices. In Figure 12, we show a cartoon of how this might work. In many ways, this hypothesis proves somewhat similar to that discussed above in section 3.2. A quasiperiodic or episodic process modulates the plasma flow, and leads to a pileup and release process that generates compressions of the piled up IMF field and drives the sawtooth oscillations we observe. In one case, reconnection produces the oscillations, while in another case ionospheric processes may generate them.

3.4. The Role of Crustal Fields

[31] Finally, crustal fields provide a natural candidate to influence the production of the sawtooth oscillations. Crustal fields affect the flow of plasma around the planetary obstacle by perturbing the location of boundaries, and also change the magnetic field draping pattern, thereby affecting many processes in the Martian magnetosphere. Most directly, they could result in pileup of interplanetary and/or induced magnetic fields, producing compressions that might launch magnetosonic waves. They also represent locations where we would expect reconnection to occur, and may affect the location of ionospheric instabilities by perturbing boundaries and/or providing an additional effective velocity shear. For draped IMF antiparallel to crustal fields, conditions favor episodic reconnection, while for draped IMF parallel to crustal fields, crustal sources can drive ionospheric instabilities by perturbing boundaries and deflecting and/or slowing the plasma flow and thereby providing additional effective velocity shear. Therefore, crustal fields could play a key role in either of the candidate mechanisms described above in sections 3.2 and 3.3, or operate on their own to produce sawtooth oscillations.

[32] Figure 13 presents a cartoon view of how this might occur. As draped field lines flow eastward around Mars, crustal fields effectively generate increased velocity shear, leading to either reconnection or instabilities that produce flux rope like features. At the same time, we see sawtooth oscillations at both poles, on field lines that pass through the subsolar region where the draped fields interact with crustal fields. This scenario suggests that some process produces compressional features, which we observe at locations downstream along the field lines (with MGS cutting through

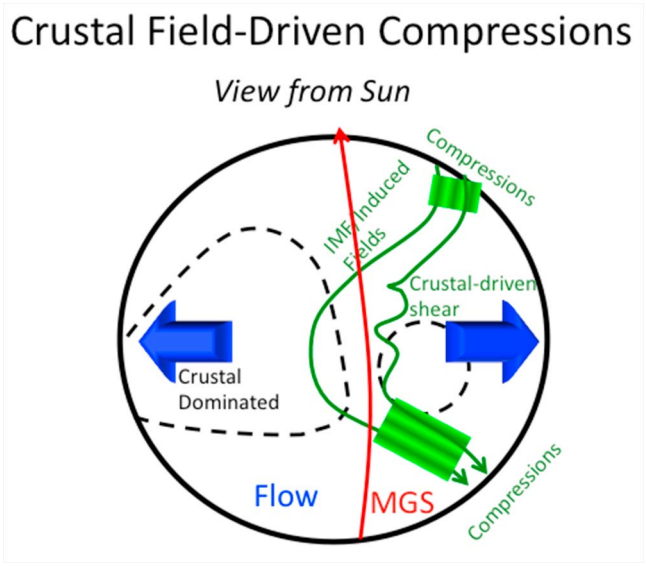

Figure 13. Schematic illustration of one possible explanation for sawtooth events shown in Figures 7 and 8, by distorted shear flows resulting from crustal fields.

these field lines only near the poles in this case). Such nonlocal effects may also help explain the seasonally varying distribution of events with respect to crustal fields.

4. Implications

[33] The observations presented in this paper, while still uncertain in origin, have implications for big picture questions at Mars. A primary scientific goal of current investigations using MGS and Mars Express data, and of the MAVEN mission now in development, is to understand the escape of planetary ions to space, including that by nonthermal ion escape mechanisms. Both reconnection and ionospheric instabilities provide a means by which solar wind and planetary plasma can cross boundaries and mix with each other, allowing bulk loss of ionized planetary gases to space. If reconnection and/or ionospheric instabilities produce the sawtooth oscillations discussed in this paper, sawtooth events could then provide an indicator for those processes at Mars. Given the frequency of observations of sawtooth oscillations, this could then indicate that those nonthermal ion escape processes operate relatively often in the Martian magnetosphere. Indeed, given the highly dynamic Mars-solar wind interaction produced by the rotation of the planet and its spatially variable crustal magnetic fields, the constantly changing solar wind conditions and IMF draping direction, and the seasonal variation of the Martian ionosphere, it would be a surprise if these dynamic processes did not play an important role at Mars. MAVEN's comprehensive plasma measurements should help differentiate between these processes, and determine their significance in the Martian environment.

[34] **Acknowledgments.** This work was supported by NASA grant NNX08AK95G. J.P.E. holds an STFC Advanced Fellowship at ICL.

[35] Masaki Fujimoto thanks the reviewers for their assistance in evaluating this manuscript.

References

Acuña, M. H., et al. (1999), Global distribution of crustal magnetization found by the Mars Global Surveyor MAG/ER experiment, *Science*, *284*, 790–793, doi:10.1126/science.284.5415.790.

Acuña, M. H., et al. (2001), The magnetic field of Mars: Summary of results from the aerobraking and mapping orbits, *J. Geophys. Res.*, *106*, 23,403–23,417, doi:10.1029/2000JE001404.

Amerstorfer, U. V., H. Gunell, N. V. Erkaev, and H. K. Biernat (2009), Shear driven waves in the induced magnetosphere of Mars: Parameter dependence, *Astrophys. Space Sci. Trans.*, *5*, 39–42, doi:10.5194/astra-5-39-2009.

Bertucci, C., C. Mazelle, D. H. Crider, D. L. Mitchell, K. Sauer, M. H. Acuña, J. E. P. Connerney, R. P. Lin, N. F. Ness, and D. Winterhalter (2004), MGS MAG/ER observations at the magnetic pileup boundary of Mars: Draping enhancement and low frequency waves, *Adv. Space Res.*, *33*, 1938–1944, doi:10.1016/j.asr.2003.04.054.

Bertucci, C., et al. (2008), The magnetic memory of Titan's ionized atmosphere, *Science*, *321*, 1475–1478, doi:10.1126/science.1159780.

Brain, D. A., F. Bagenal, M. H. Acuña, J. E. P. Connerney, D. H. Crider, C. Mazelle, D. L. Mitchell, and N. F. Ness (2002), Observations of low-frequency electromagnetic plasma waves upstream from the Martian shock, *J. Geophys. Res.*, *107*(A6), 1076, doi:10.1029/2000JA000416.

Brain, D. A., J. S. Halekas, R. J. Lillis, D. L. Mitchell, R. P. Lin, and D. H. Crider (2005), Variability of the altitude of the Martian sheath, *Geophys. Res. Lett.*, *32*, L18203, doi:10.1029/2005GL023126.

Brain, D. A., R. J. Lillis, D. L. Mitchell, J. S. Halekas, and R. P. Lin (2007), Electron pitch angle distributions as indicators of magnetic field topology near Mars, *J. Geophys. Res.*, *112*, A09201, doi:10.1029/2007JA012435.

Brain, D. A., A. H. Baker, J. Briggs, J. P. Eastwood, J. S. Halekas, and T.-D. Phan (2010), Episodic detachment of Martian crustal magnetic fields leading to bulk atmospheric plasma escape, *Geophys. Res. Lett.*, *37*, L14108, doi:10.1029/2010GL043916.

Cain, J. C., B. B. Ferguson, and D. Mozzoni (2003), An n = 90 internal potential function of the Martian crustal magnetic field, *J. Geophys. Res.*, *108*(E2), 5008, doi:10.1029/2000JE001487.

Dubinin, E., K. Sauer, K. Baumgärtel, and K. Srivastava (1998), Multiple shocks near Mars, *Earth Planets Space*, *50*, 279–287.

Dubinin, E., M. Franz, J. Woch, E. Roussos, S. Barabash, R. Lundin, J. D. Winningham, R. A. Frahm, and M. Acuña (2006), Plasma morphology at Mars. ASPERA-3 observations, *Space Sci. Rev.*, *126*, 209–238, doi:10.1007/s11214-006-9039-4.

Dubinin, E., et al. (2008a), Structure and dynamics of the solar wind/ionosphere interface on Mars: MEX-ASPERA-3 and MEX-MARSIS observations, *Geophys. Res. Lett.*, *35*, L11103, doi:10.1029/2008GL033730.

Dubinin, E., et al. (2008b), Plasma environment of Mars as observed by simultaneous MEX-ASPERA-3 and MEX-MARSIS observations, *J. Geophys. Res.*, *113*, A10217, doi:10.1029/2008JA013355.

Duru, F., D. A. Gurnett, R. A. Frahm, J. D. Winningham, D. D. Morgan, and G. G. Howes (2009), Steep, transient density gradients in the Martian ionosphere similar to the ionopause at Venus, *J. Geophys. Res.*, *114*, A12310, doi:10.1029/2009JA014711.

Eastwood, J. P., D. A. Brain, J. S. Halekas, J. F. Drake, T. D. Phan, M. Øieroset, D. L. Mitchell, R. P. Lin, and M. Acuña (2008), Evidence for collisionless magnetic reconnection at Mars, *Geophys. Res. Lett.*, *35*, L02106, doi:10.1029/2007GL032289.

Espley, J. R., P. A. Cloutier, D. A. Brain, D. H. Crider, and M. H. Acuña (2004), Observations of low-frequency magnetic oscillations in the Martian magnetosheath, magnetic pileup region, and tail, *J. Geophys. Res.*, *109*, A07213, doi:10.1029/2003JA010193.

Fairfield, D. H., A. Otto, T. Mukai, S. Kokubun, R. P. Lepping, J. T. Steinberg, A. J. Lazarus, and T. Yamamoto (2000), Geotail observations of the Kelvin-Helmholtz instability at the equatorial magnetotail boundary for parallel northward fields, *J. Geophys. Res.*, *105*, 21,159–21,173, doi:10.1029/1999JA000316.

Gunell, H., et al. (2008), Shear driven waves in the induced magnetosphere of Mars, *Plasma Phys. Controlled Fusion*, *50*, doi:10.1088/0741-3335/50/7/074018.

Gurnett, D. A., D. D. Morgan, F. Duru, F. Akalin, J. D. Winningham, R. A. Frahm, E. Dubinin, and S. Barabash (2009), Large density fluctuations in the Martian ionosphere as observed by the Mars Express radar sounder, *Icarus*, *206*, 83–94, doi:10.1016/j.icarus.2009.02.019.

Halekas, J. S., J. P. Eastwood, D. A. Brain, T. D. Phan, M. Øieroset, and R. P. Lin (2009), In situ observations of reconnection Hall magnetic fields at Mars: Evidence for ion diffusion region encounters, *J. Geophys. Res.*, *114*, A11204, doi:10.1029/2009JA014544.

Krymskii, A. M., T. K. Breus, N. F. Ness, M. H. Acuña, J. E. P. Connerney, D. H. Crider, D. L. Mitchell, and S. J. Bauer (2002), Structure of the magnetic field fluxes connected with crustal magnetization and topside

ionosphere at Mars, *J. Geophys. Res.*, *107*(A9), 1245, doi:10.1029/2001JA000239.

Mitchell, D. L., R. P. Lin, C. Mazelle, H. Rème, P. A. Cloutier, J. E. P. Connerney, M. H. Acuna, and N. F. Ness (2001), Probing Mars' crustal magnetic field and ionosphere with the MGS Electron Reflectometer, *J. Geophys. Res.*, *106*, 23,419–23,427, doi:10.1029/2000JE001435.

Nagy, A. F., et al. (2004), The plasma environment of Mars, *Space Sci. Rev.*, *111*, 33, doi:10.1023/B:SPAC.0000032718.47512.92.

Otto, A., and D. H. Fairfield (2000), Geotail observations of the Kelvin-Helmholtz instability at the equatorial magnetotail boundary for parallel northward fields, *J. Geophys. Res.*, *105*, 21,175–21,190, doi:10.1029/1999JA000312.

Penz, T., et al. (2004), Ion loss on Mars caused by the Kelvin-Helmholtz instability, *Planet. Space Sci.*, *52*, 1157–1167, doi:10.1016/j.pss.2004.06.001.

Sundberg, T., S. A. Boardsen, J. A. Slavin, L. G. Blomberg, and H. Korth (2010), The Kelvin-Helmholtz instability at Mercury: An assessment, *Planet. Space Sci.*, *58*, 1434–1441, doi:10.1016/j.pss.2010.06.008.

Tsurutani, B. T., R. M. Thorne, E. J. Smith, J. T. Gosling, and H. Matsumoto (1987), Steepened magnetosonic waves at comet Giacobini-Zinner, *J. Geophys. Res.*, *92*, 11,074–11,082, doi:10.1029/JA092iA10p11074.

Winningham, J. D., et al. (2006), Electron oscillations in the induced Martian magnetopause, *Icarus*, *182*, 360–370, doi:10.1016/j.icarus.2005.10.033.

D. A. Brain and J. S. Halekas, Space Sciences Laboratory, 7 Gauss Way, University of California, Berkeley, CA 94720, USA. (jazzman@ssl.berkeley.edu)

J. P. Eastwood, Blackett Laboratory, Imperial College London, London SW7 2AZ, UK.